

An Unsteady Flow and Nonlinear Radiative Heat Transfer of Nanofluid over a Stretching Sheet

Dr. M.R.Krishnamurthy

Department of Mathematics,
JNN College of Engineering,
Shivamogga – 577204
Karnataka, INDIA.
E-mail:krishnamr@jnnce.ac.in

Dr. B.J.Gireesha

Department of Studies and Research in
Mathematics,
Kuvempu University,
Shankaraghatta-577 451,
Shimoga, Karnataka, INDIA.

Abstract: This paper investigates the slip flow and nonlinear radiative heat transfer of nanofluid over an unsteady stretching sheet in a porous medium in the presence of chemical reaction. The governing equations are transformed to ordinary differential equations by using similarity transformation. Numerical solutions of these equations are obtained by using the Runge-Kutta-Fehlberg-45 order method with Shooting Technique. The effects of non-dimensional governing parameters on the velocity, temperature, concentration profiles are discussed and presented through graphs and tables. Accuracy of the results compared with the existing ones. Excellent agreement is found with earlier studies.

Keywords: Boundary layer flow, velocity slip, nonlinear thermal radiation, chemical reaction, numerical solution.

Nomenclature:

(u, v) : velocity components along the x and y axis,
 ρ : density of the nanofluid,
 $\alpha = \frac{k}{(\rho c)_f}$: nanofluid thermal diffusivity,
 ν : kinematic viscosity,
 D_B : Brownian diffusion coefficient,
 D_T : thermophoresis diffusion coefficient,
 T : nanofluid temperature,

θ : Non-dimensional temperature,
 $(\rho c)_f$: heat capacity of the fluid,
 $(\rho c)_p$: effective heat capacity of the nanoparticle,
 q_r : Radiative heat flux,
 $k' = \frac{k^*}{1-\alpha\tau}$: is the nonuniform permeability of the porous medium,
 $\tau = \frac{(\rho c)_p}{(\rho c)_f}$: ratio between the effective heat capacity of the nanoparticle material and the fluid,
 k_0 : chemical reaction coefficient,
 C : volumetric volume expansion coefficient,
 T_w : temperature of the nanofluid near wall,
 T_∞ : free stream temperature of the nanofluid,
 k : thermal conductivity,
 $U_w(x, t) = \frac{bx}{1-\alpha t}$: stretching sheet velocity,
 b : is the initial stretching rate,
 α : is the positive constant which measures the unsteadiness,
 $\frac{b}{1-\alpha t}$: in the initial stretching rate that increases with time,
 $N_1 = N(1-\alpha t)^{\frac{1}{2}}$: velocity slip factor,
 $c = N\sqrt{bx}$: velocity slip parameter,
 $k_p = \frac{\nu}{k^*}$: permeability parameter,

$Pr = \frac{\nu}{\alpha}$: Prandtl number,

$Nr = \frac{16\sigma^*T_w^3}{3k\kappa^2}$: Radiation parameter,

$Nb = \frac{\tau D_B (C_w - C_\infty)}{\nu}$: Brownian motion

parameter,

$Nt = \frac{\tau D_T (T_w - T_\infty)}{\nu T_\infty}$: thermophoresis parameter,

$Le = \frac{\nu}{D_B}$: Lewis number,

$\gamma = \frac{k_1 C_w}{\alpha}$: chemical reaction parameter,

C_f : local skin friction coefficient,

Nu_w : local Nusselt number,

Sh_w : Sherwood number,

Re_x : local Reynolds number.

1. Introduction

Nanofluid is a new dynamic subclass of nanotechnology-based heat transfer fluids obtained by dispersing and stably suspended nanoparticles with typical dimensions of shape and size 1-100 nm. Choi and Eastman [1] refers to the dispersions of nanometer-sized particles in a base fluid such as water, ethylene glycol and propylene glycol, to increase their thermal conductivities. Radiation effect of a water-based nanofluid flow on a boundary layer flow with variable viscosity due to a heated convective stretching sheet was observed by Makinde and Mishra [2]. Bachok et al. [3] analyzed the unsteady boundary-layer flow and heat transfer of a nanofluid over a permeable stretching sheet. Later on, a two dimensional MHD flow of nanofluids on a stretching plate by the cause of radiation, velocity, and thermal slip boundary conditions was investigated by Pal and Mandal [4]. A flow on a boundary layer and heat transport properties under the impact of slip velocity, Brownian motion, and thermal radiation were considered by Pal and Roy [5]. Experimental and theoretical studies on convective heat transfer in nanofluids and their applications has been presented by Godson et al. [6]. In recent years, many researchers have studied and reported nanofluid technology experimentally or numerically in the presence of heat transfer [7-13].

The boundary layer flow and heat transfer in a quiescent fluid driven by a continuous stretching sheet is of significance in a

number of industrial engineering processes, such as drawing of a polymer sheet or filaments extruded continuously from a die, cooling of a metallic plate in a bath, aerodynamic extrusion of plastic sheets, continuous casting, rolling, annealing and tinning of copper wires, wire and fiber coating, etc. During the processes, mechanical properties are greatly dependent upon the rate of cooling. The classical problem of steady flow on a stretched surface extruded from a slit was first considered by Sakiadis [14, 15], who developed a numerical solution using a similarity transformation. Erickson et al. [16] have extended the work of Sakiadis [14] by employing fluid suction or injection at the stretched wall and investigating its effects on the heat and mass transfer within the boundary layer. Crane [17] initiated the analytical study of boundary layer flow of a Newtonian fluid over a linearly stretching surface. The problem of steady flow past a stretching surface has been extended by many authors [18-20]. All of the above-mentioned studies were restricted in the steady state conditions. The transient or unsteady aspects become interesting in certain practical problems where the motion of the stretched surface may start impulsively from rest.

Nevertheless, in many engineering applications, unsteadiness becomes an integral part of the problem where the flow becomes time-dependent [21, 22, 23]. Thus, motivated by this, we extend the study of Bachok et al. [3] to the case of convective surface boundary condition. For a long time,

constant surface temperature and heat flux are customarily used. However, there are times when heat transfer at the surface relies on the surface temperature, as what mostly occurs in heat exchangers. In this situation, convective boundary condition is used to replace the condition of prescribed surface temperature. Makinde and Aziz[24] have studied the Boundary layer flow of a nanofluid past a stretching sheet with a convective boundary condition. Unsteady boundary layer flow of a nanofluid over a stretching/shrinking sheet with a convective boundary condition was studied by Syahira Mansur and Anuar Ishak[25]. Pal [26] investigated the unsteady convective boundary layer flow and heat transfer over a stretching surface with non-uniform heat source/sink and thermal radiation. Kalidas Das et al. [27] investigated the unsteady boundary layer flow of a nanofluid over a heated stretching sheet with thermal radiation. Daniel [28] focuses on the effects of suction as well as thermal radiation, chemical reaction, viscous dissipation and Joule heating on a two-dimensional natural convective flow of unsteady electrical magnetohydrodynamic nanofluid over a linearly permeable stretching sheet.

In the above mentioned studies were confined to the linear approximation for the radiative heat transfer effects which are valid for small temperature differences. It is difficult to construct a system in scientific and engineering applications in which the working fluids will have a small temperature differences. Therefore, the heat transfer with nonlinear radiation has been recently presented by some researchers. The Sakiadis flow with nonlinear Rosseland thermal radiation was considered by Pantokratoras and Fang [29]. Unlike, small temperature difference within the fluid, they have assumed large temperature differences within the fluid. Cortell [30] discussed the fluid flow and radiative nonlinear heat transfer over a stretching sheet. Recently, Mushtaq et al. [31] studied a nonlinear radiative heat transfer in the flow of

nanofluid due to solar energy. Hayat et al. [32] analyzed the magneto hydro dynamic three-dimensional flow of viscoelastic nanofluid in the presence of nonlinear thermal radiation. Very recently, Prasannakumara et al. [33] investigated the effects of chemical reaction and nonlinear thermal radiation on Williamson nanofluid slip flow over a stretching sheet embedded in a porous medium.

To the authors' knowledge no studies have been reported on the slip effect on boundary layer flow and heat transfer of nanofluid over an unsteady stretching sheet in a porous medium by considering nonlinear thermal radiation and chemical reaction. In this study the governing equations are transformed to ordinary differential equations by using similarity transformation. Numerical solutions of these equations are obtained by using the Runge-Kutta-Fehlberg-45 order method along with Shooting Technique. The effects of non-dimensional governing parameters on the velocity, temperature, concentration profiles, friction factor, Nusselt and Sherwood numbers are discussed and presented through graphs and tables. Accuracy of the results to the existing ones and are found to be in excellent agreement with earlier studies.

2. Mathematical Formulation

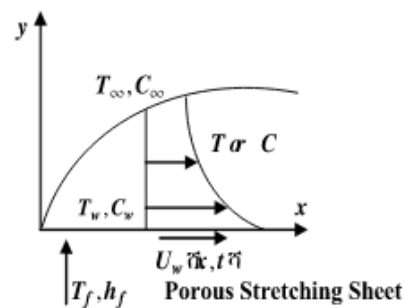


Fig.1: Schematic representation of boundary layer flow.

Consider an unsteady, incompressible, electrically conducting, two dimensional boundary layer flow of a dissipative nanofluid past a stretching sheet with non-

uniform velocity $U_w(x, t)$ and permeability k' . The x -axis is along the continuous stretching surface and y axis is normal to the surface. The boundary layer equations that

govern the present flow subject to the Boussinesq approximation can be expressed as

$$\frac{\partial u}{\partial x} + \frac{\partial v}{\partial y} = 0, \tag{2.1}$$

$$\frac{\partial u}{\partial t} + u \frac{\partial u}{\partial x} + v \frac{\partial u}{\partial y} = \nu \frac{\partial^2 u}{\partial y^2} - \frac{\nu}{k} u, \tag{2.2}$$

$$\frac{\partial T}{\partial t} + u \frac{\partial T}{\partial x} + v \frac{\partial T}{\partial y} = \alpha \frac{\partial^2 T}{\partial y^2} + \tau \left[D_B \frac{\partial C}{\partial y} \frac{\partial T}{\partial y} + \frac{D_T}{D_m} \left(\frac{\partial T}{\partial y} \right)^2 \right] - \frac{1}{(\rho c)_f} \frac{\partial q_r}{\partial y}, \tag{2.3}$$

$$\frac{\partial C}{\partial t} + u \frac{\partial C}{\partial x} + v \frac{\partial C}{\partial y} = D_B \frac{\partial^2 C}{\partial y^2} + \frac{D_T}{D_m} \frac{\partial^2 T}{\partial y^2} - k_0(C - C_\infty), \tag{2.4}$$

The Boundary conditions for the model as follows

$$u = U_w(x, t) + N_1 v \left(\frac{\partial u}{\partial y} \right), \quad v = 0, \quad -k_f \frac{\partial T}{\partial y} = h_f(T_f - T), \quad C = C_w \text{ at } y = 0, \\ u = 0, \quad T = T_\infty, \quad C = C_\infty \text{ as } y \rightarrow \infty. \tag{2.5}$$

Unlike the linearized Rosseland approximation, we use nonlinear Rosseland diffusion approximation from which one can obtain results for both small and large

differences between T_w and T_∞ . Using Rosseland approximation for radiation, the radiative heat flux is simplified as,

$$q_r = - \frac{4\sigma^* \partial T^4}{3k^* \partial y}, \tag{2.6}$$

For a boundary layer flow over a horizontal flat plate (Pantokratoras and Fang, [29]), from Eq. (2.6) we get,

$$q_r = \left(- \frac{16\sigma^* T_\infty^3}{3k^*} \right) \frac{dT}{dy}, \tag{2.7}$$

In view to Eq. (2.8), energy equation(2.3) takes the form

$$\frac{\partial T}{\partial t} + u \frac{\partial T}{\partial x} + v \frac{\partial T}{\partial y} = \frac{\partial}{\partial y} \left[\left(\alpha + \frac{16\sigma^* T_\infty^3}{3k^* (\rho c)_f} \right) \frac{\partial T}{\partial y} \right] + \frac{\rho_m c_m}{(\rho c)_f} \left[D_B \frac{\partial C}{\partial y} \frac{\partial T}{\partial y} + \frac{D_T}{D_m} \left(\frac{\partial T}{\partial y} \right)^2 \right], \tag{2.8}$$

For similarity solution, we introduce the following similarity transformation

$$\eta = \sqrt{\frac{b}{1-\alpha t}} y, \quad \psi(x, y) = \sqrt{\frac{b\nu}{1-\alpha t}} x f(\eta), \quad \theta(\eta) = \frac{T - T_\infty}{T_f - T_\infty}, \quad \phi(\eta) = \frac{C - C_w}{C_w - C_\infty}, \\ T = T_w(x, t) = T_\infty + \left(\frac{b\nu}{1-\alpha t} \right) \theta(\eta), \quad C = C_w(x, t) = C_\infty + \left(\frac{b\nu}{1-\alpha t} \right) \phi(\eta), \tag{2.9}$$

Where $\psi(x, y)$ is a stream function which satisfies the continuity equation (2.1) with

$$u = \frac{bW}{(1-\alpha\tau)} f'(\eta), \quad v = \sqrt{\frac{bW}{1-\alpha\tau}} f(\eta). \quad (2.10)$$

Using equations (2.9) and (2.10), equations (2.2), (2.4) and (2.8) becomes

$$f'''' + ff'' - (f')^2 - \frac{4}{2}\eta f'' - (A + k_p)f' = 0, \quad (2.11)$$

$$\left[1 + Nr(1 + (\theta_w - 1)\theta)^2\theta'\right] + Pr \left[f\theta' - f'\theta - A\left(\theta + \frac{1}{2}\eta\theta'\right) + Nb\theta'\phi' + Nt(\theta')^2 + Ec(f'')^2\right]. \quad (2.12)$$

$$\phi'' + Le \left[f\phi' - f'\phi - A\left(\phi + \frac{1}{2}\eta\phi'\right)\right] + \frac{Ni}{Nb}\theta'' - \gamma\phi = 0. \quad (2.13)$$

Subject to the boundary conditions,

$$f(0) = 0, \quad f'(0) = 1 + \epsilon f''(0), \quad \theta'(0) = -Bi(1 - \theta(0)), \quad \phi(0) = 1,$$

$$f'(\infty) = 0, \quad \phi(\infty) = 0, \quad \theta(\infty) = 0. \quad (2.14)$$

For engineering interest the skin-friction coefficient, the reduced Nusselt number, and the reduced Sherwood numbers are given by,

$$\frac{1}{2}(Re_w)^{\frac{1}{2}} = f''(0), \quad \frac{Nu_w}{\sqrt{Re_w}} = -(1 + Nr\theta_w^2)\theta'(0), \quad \frac{Sh_w}{\sqrt{Re_w}} = -\phi'(0). \quad (2.15)$$

where, $Re_w = \frac{\rho U_w(x) x}{\mu}$ is the local Reynold's number.

3. Numerical Procedure

The system of Eqs. (2.11) to (2.13) with boundary conditions of (2.14) has been solved by employing a reputable numerical Runge–Kutta–Fehlberg (RKF-45) method coupled with the shooting technique. For the solution

of the problem, shooting method converts the system to a set of initial value problems and then solution is obtained by RKF-45 method. The step size is taken as 0.001, and

the convergence criteria are taken as 10^{-6} . It is pertinent to mention here that all the results in this study have been computed by using the mathematical software Maple. The values of Nusselt number and Sherwood number for different parameters was shown in Table 1 and Table 2, respectively for the cases of unsteady and steady flow with linear and nonlinear Rosseland approximations.

4. Results and discussion

This section is dedicated to check and plot the influence of various parameters on

velocity, temperature and concentration profiles. Figs.2 and 3 shows the effect of velocity and temperature, concentration profile respectively for various values of unsteady parameter (A). From these figures we observed that for increasing values of A velocity and temperature, concentration profile decreases. We may explain this phenomenon as increase in unsteady parameter improves the temperature near the stretching sheet. This makes the wall temperature is higher than the ambient temperature, and due to this high wall temperature nano particles move to cooler area, causing a decline in the concentration profiles also.

Figs.4 and 5 respectively illustrate the effect of the velocity slip parameter (c) on velocity and temperature, nanoparticles volume fraction profiles. We can observe that the effect of increasing value of velocity slip parameter reduces the thickness of momentum boundary layer and hence decrease the velocity. By this we meant that the velocity slip coefficient corresponds to increase in both temperature and concentration profile. This must be due to the existence of slip velocity on the stretching surface.

Figs.6 and 7 illustrates the effect of permeability parameter (k_p) on velocity and temperature, concentration profiles. It is obvious that the presence of porous medium causes higher restriction to the fluid flow which, in turn, slows its motion. Therefore, with an increase in permeability parameter, the resistance to the fluid motion increases and hence velocity decreases as result of this temperature and concentration increases.

In Fig.8, the variation of temperature $\theta(\eta)$ with η for various values of the Biot number (B_f) is presented. It is observed that temperature field $\theta(\eta)$ increases rapidly near the boundary by increasing Biot number. This is because of convective heat exchange at the plate surface leading to an increase in thermal boundary layer thickness.

Fig.9 is plotted for the temperature distribution for different values of Eckert number (E_c). We observe that the effect of increasing values of Eckert number is to increase the temperature. Further it is noticed from this graph that the effect of viscous dissipation is to amplify the temperature. This is due to fact that heat energy is stored in the fluid due to the frictional heating.

Figs.10 and 11 indicate that temperature increases by increasing values of radiation parameter (N_r) and temperature ratio parameter (θ_w), physically this is due to the fact that with the increase in radiation parameter, the absorption coefficient decreases. Hence the rate of radiative heat transfer to the fluid increases. Increase in radiation parameter, the mean absorption coefficient decreases. Hence the rate of radiative heat transfer to the fluid increases.

The effect of chemical reaction parameter (γ) on nanoparticle volume fraction profile is depicted in Fig.12 for species consumption and generation cases. It is observed that the nanoparticles volume fraction decreases for constructive chemical reaction parameter and increases for destructive chemical reaction parameter on stretching surface.

Fig.13 shows that the temperature profile increases but nanoparticles volume fraction profile decreases for higher values of Brownian motion parameter (Nb) and is due to higher thermal conductivity of the nanofluid. Both temperature and nanoparticles volume fraction exhibits an increasing nature for larger values of thermophoresis parameter (Nt) (See Fig.14) By this we meant that both $\theta(\eta)$ and $\phi(\eta)$ are directly proportional to the thermophoresis parameter.

Figs.15 and 16 displays the effect of Lewis number (Le) on concentration and temperature profiles. From these figures the concentration profiles decrease with increasing the values of the Le . It is due to

the fact that the larger values of Lewis number makes the mass diffusivity smaller, therefore it decreases the concentration field. The temperature profile increases for increasing the values of Le .

Fig.17 depicts the effect of Prandtl number (Pr) on temperature profiles. In the presence of slip and Biot number, an increase in Prandtl number decreases the temperature profiles.

5. Conclusion

In the present paper, we have studied numerically as well as physically the slip flow and nonlinear radiative heat transfer on nanofluid past a unsteady stretching sheet embedded in a porous medium with chemical reaction. From the present investigation, the following conclusions are:

- The velocity, temperature and nanoparticle volume fraction profiles decrease with the increase in the value of the unsteadiness parameter.
- For increasing the values of velocity slip parameter, decreases the velocity profile whereas the reverse trend is seen for temperature profile.
- Temperature profile increases for increasing the values of Biot number, Eckert number, radiation parameter and temperature ratio parameter whereas the reverse trend is seen for Prandtl number.
- There is an appreciable increase in the nanoparticles concentration and rate of mass transfer at the sheet when the strength of thermophoretic effect is increased.

References:

1. S.U.S. Choi, J.A. Eastman, Enhancing thermal conductivities of fluids with nanoparticles, in: Proceedings of the 1995 ASME International Mechanical Engineering Congress and Exposition, San Francisco, (1995).
2. O. D. Makinde and S. R. Mishra, "On stagnation point flow of variable viscosity nanofluids past a stretching surface with radiative heat," *Int. J. Appl. Comput. Math.*, 2017, 3: 561-578.
3. N. Bachok, A. Ishak, I. Pop, Unsteady boundary-layer flow and heat transfer of a nanofluid over a permeable stretching/shrinking sheet, *Int. J. Heat Mass Transf.*, 55: (2012) 2102–2109.
4. D. Pal and G. Mandal, "Influence of Lorentz force and thermal radiation on heat transfer of nanofluids over a stretching sheet with velocity–thermal slip," *Int. J. Appl. Comput. Math.*, 2017, 3(4): 3001-3020.
5. D. Pal and N. Roy, "Influence of Brownian motion and thermal radiation on heat transfer of a nanofluid over a stretching sheet with slip velocity," *Int. J. Appl. Comput. Math.*, 2017, 3(4): 3355–3377.
6. D. Godson, D. Raja, S. Mohan Lal and Wongwises, Enhancement of heat transfer using nanofluids- an overview, *Renew Sustain Energy Rev.*, 14: (2010) 629–641.
7. J. Buongiorno, Convective transport in nanofluids, *J. Heat Transf.*, 128: (2006) 240–250.
8. D.A. Nield and A.V. Kuznetsov, Thermal instability in a porous medium layer saturated by a nanofluid, *Int. J. Heat Mass Transf.*, 52: (2009) 5796–5801.
9. N. Bachok, A. Ishak and I. Pop, Unsteady boundary-layer flow and heat transfer of a nanofluid over a permeable stretching/shrinking sheet, *Int. J. Heat Mass Transf.*, 55 (2012) 2102–2109.
10. M.R. Krishnamurthi, B.C. Prasannakumara, B.J. Gireesha and Rama Subba Reddy Gorla, Effect of chemical reaction on MHD boundary layer flow and melting heat transfer of Williamson nanofluid in porous medium, *Engineering Science and Technology, an International Journal*, 19: (2016) 53–61.
11. B.C. Prasannakumara, B.J. Gireesha, M.R. Krishnamurthy and K. Ganesh Kumar, MHD flow and nonlinear radiative heat transfer of Sisko nanofluid

- over a nonlinear stretching sheet, *Informatics in Medicine Unlocked*, 9: (2017) 123–132.
12. M.R. Krishnamurthy, B.J. Gireesha, B.C. Prasannakumara and Rama Subba Reddy Gorla, Thermal radiation and chemical reaction effectson boundary layer slip flow and melting heat transfer of nanofluid induced by a nonlinear stretching sheet, *Nonlinear Engineering*, 2016; aop DOI 10.1515/nleng-2016-0013
 13. M. Qasim, Z. H. Khan, R. J. Lopezand W. A. Khan, Heat and mass transfer in nanofluid thin film over an unsteady stretching sheet using Buongiorno's model, *The European Physical Journal Plus*, 131: (2016) 16.
 14. B.C.Sakiadis, Boundary layer behavior on continuous solid surfaces: i. boundary layer equations for two-dimensional and axisymmetric flow, *AIChE J.*, 7: (1961) 26–28.
 15. B.C. Sakiadis, Boundary layer behavior on continuous solid surfaces: ii. the boundary layer on a continuous flat surface, *AIChE J.* 7: (1961) 221–225.
 16. L.E. Erickson,L.T.Fan and V.G. Fox, Heat and mass transfer on moving continuous flat plate with suction or injection, *Ind. Eng. Chem. Fund.*, 5: (1966) 19–25.
 17. L.J.Crane,Flows past a stretching plate, *Z. Angew. Math. Phys. (ZAMP)*, 21: (1970) 645–647.
 18. M.E. Ali, Heat transfer characteristics of a continuous stretching surface, *Wärme - und Stoffübertragung*, 29(4): (1994) 227–234.
 19. T. Fang, S. Yao, J. Zhang and A. Aziz, Viscous flow over a shrinking sheet with a second order slip flow model, *Commun. Nonlinear Sci. Numer. Simul.*, 15: (2010) 1831–1842.
 20. K. Zaimi, A. Ishak and I. Pop, Boundary layer flow and heat transfer past a permeable shrinking sheet in a nanofluid with radiation effect, *Adv. Mech. Eng.*, 2012: (2012) 1–7 Article ID 340354.
 21. M. Khan and Hashim, Boundary layer flow and heat transfer to Carreau fluid over a nonlinear stretching sheet, *AIP Advances*, 5: (2015) 107203.
 22. M. Mustafa, T. Hayat and A. Alsaedi, Unsteady boundary layer flow of nanofluid past an impulsively stretching sheet, *Journal of Mechanics*, 29(3): (2013).
 23. M. Ferdows, S.M. Chapa, and A.A. Afify, Boundary layer flow and heat transfer of a nanofluid over a permeable unsteady stretching sheet with viscous dissipation, *Journal of Engineering Thermophysics*, 23(3): (2014) 216–228.
 24. O.D. Makinde and A. Aziz , Boundary layer flow of a nanofluid past a stretching sheet with a convective boundary condition, *Int. J. Therm. Sci.*, 50: (2011) 1326–1332 .
 25. S. Mansur and A.Ishak, Unsteady boundary layer flow of a nanofluid over a stretching/shrinking sheet with a convective boundary condition, *Journal of the Egyptian Mathematical Society*, (2016)
 26. Dulal Pal,Unsteady convective boundary layer flow and heat transfer over a stretching surface with non-uniform heat source/sink and thermal radiation, *International Journal for Computational Methods in Engineering Science and Mechanics*, 16 (3): (2015).
 27. Kalidas Das, P.R.Duari, P.K. Kundu, Nanofluid flow over an unsteady stretching surface in presence of thermal radiation, *Alexandria Engineering Journal*, (2014) 53: 737–745.
 28. Y.S. Daniel, Z.A. Aziz, Z. Ismail and F. Salah, Thermal radiation on unsteady electrical MHD flow of nanofluid over stretching sheet with chemical reaction *Journal of King Saud University – Science*, xxx (2017).
 29. A. Pantokratoras and T. Fang, Sakiadis flow with nonlinear Rosseland thermal radiation, *Physic Scrip*, 87(1): (2013) 5 pages.

30. R. Cortell, Fluid flow and radiative nonlinear heat transfer over a stretching sheet, *J. King Saud University-Sci.*, 26: (2014) 161-167.
31. A. Mushtaq, M. Mustafa, T. Hayat and A. Alsaedi, Nonlinear radiative heat transfer in the flow of nanofluid due to solar energy, *J. Taiwan Inst. Chem. Eng.*, 45(54): (2014) 1176-1183.
32. T. Hayat, Taseer Muhammada, A. Alsaedi and M.S. Alhuthali, Magnetohydrodynamic three-dimensional flow of viscoelastic nanofluid in the presence of nonlinear thermal radiation, *J. Magnetism and Magnetic Materials*, 385: (2015) 222–229.
33. B.C. Prasannakumara, B.J. Gireesha, Rama Subba Reddy Gorla and M.R. Krishnamurthy, Effects of chemical reaction and nonlinear thermal radiation on Williamson nanofluid slip flow over a stretching sheet embedded in a porous medium, *Journal of Aerospace Engineering*, 29: (2016) pp. 04016019.

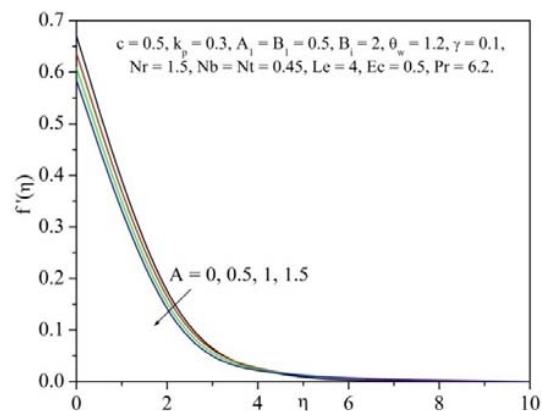


Fig.2: Velocity profile for various values of unsteady parameter A .

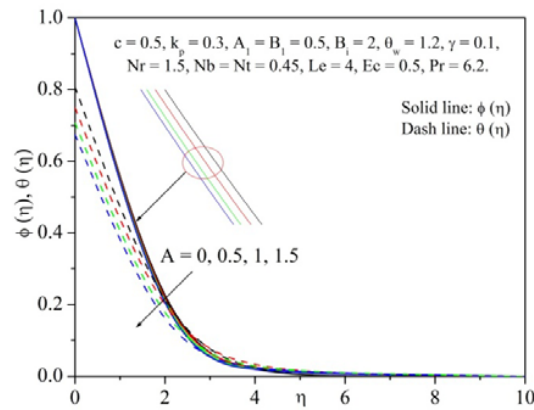


Fig.3: Temperature and concentration profile for various values of unsteady parameter A .

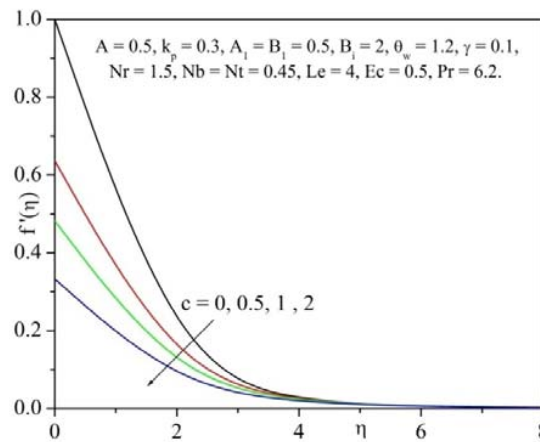


Fig.4: Velocity profile for various values of velocity slip parameter c .

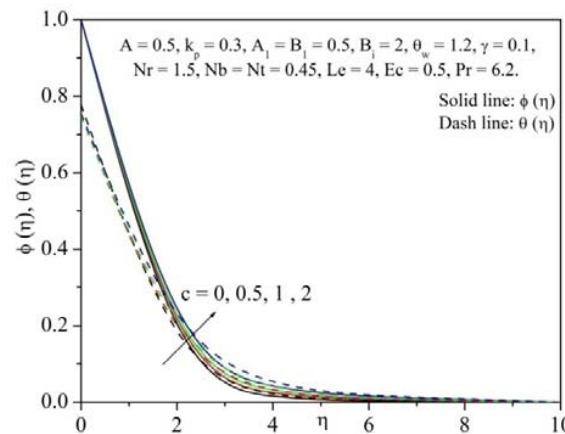


Fig.5: Temperature and concentration profile for various values of velocity slip parameter c .

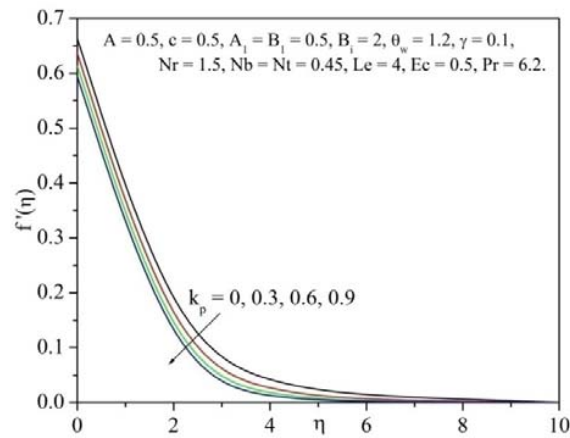


Fig.6: Velocity profile for various values of permeability parameter k_p .

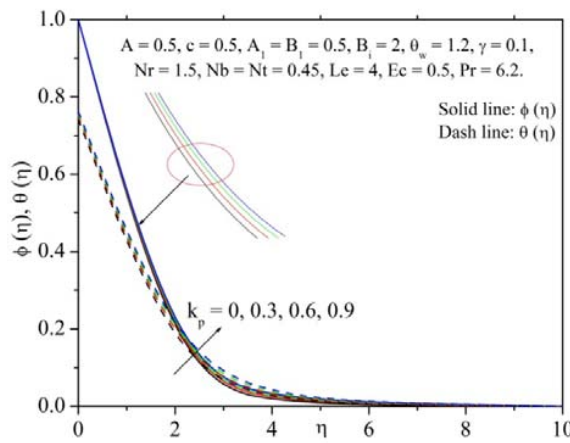


Fig.7: Temperature and concentration profile for various values of permeability parameter k_p .

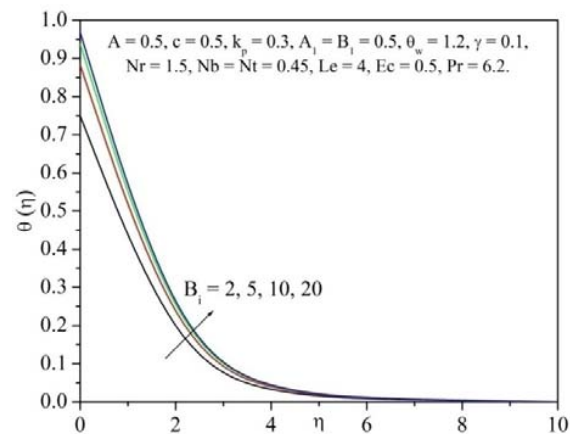


Fig.8: Temperature profile for various values of Biotnumber B_1 .

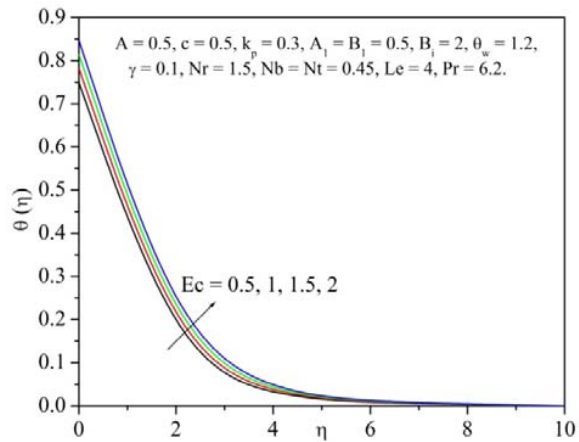


Fig.9: Temperature profile for various values of Eckert number Ec .

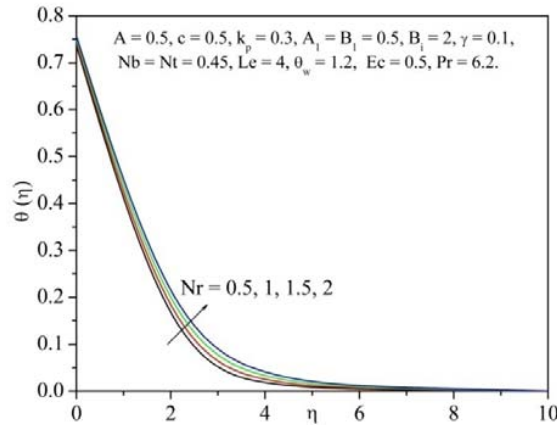


Fig.10: Temperature profile for various values of Radiation parameter Nr .

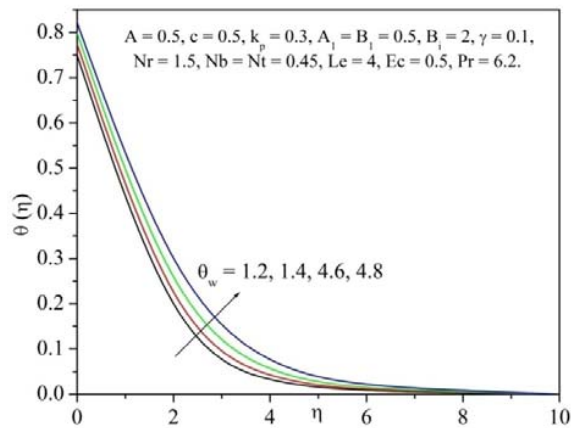


Fig.11: Temperature profile for various values of temperature ratio parameter θ_w .

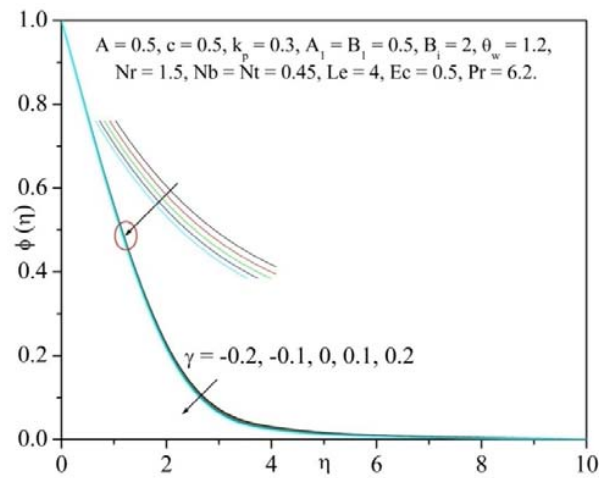


Fig.12: Concentration profile for various values of chemical reaction parameter γ .

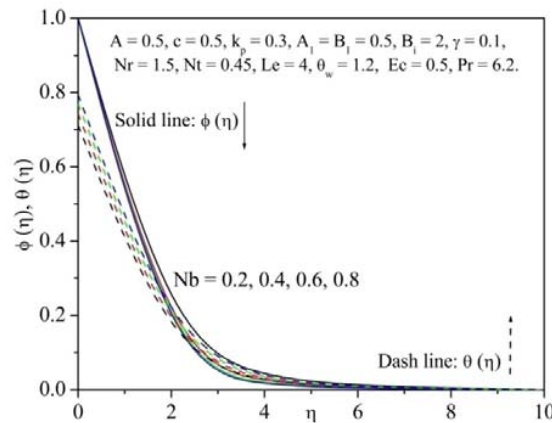


Fig.13: Temperature and concentration profile for various values of Brownian motion parameter Nb .

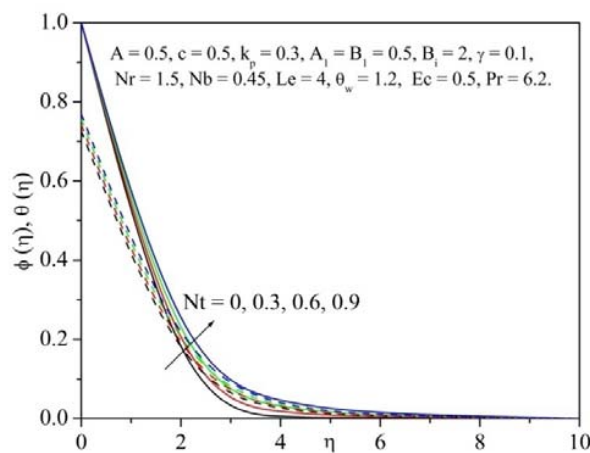


Fig.14: Temperature and concentration profile for various values of Thermophoresis parameter Nt .

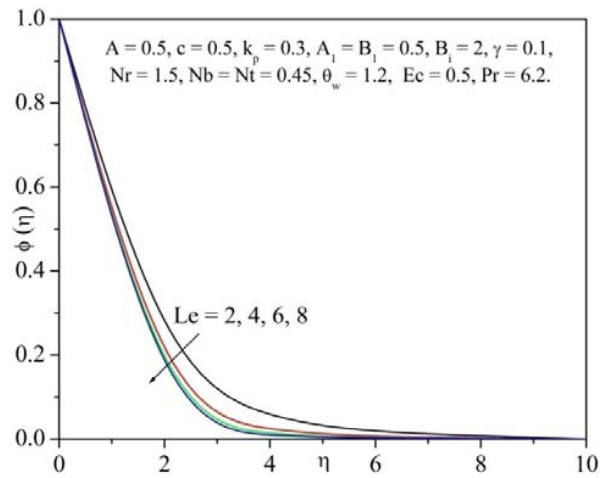


Fig.15: Concentration profile for various values of Lewis number Le .

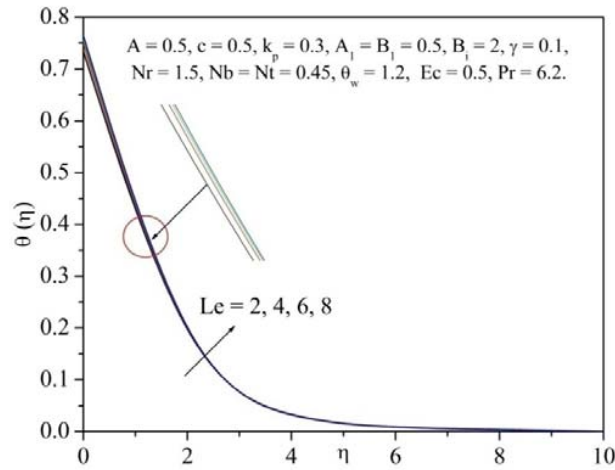


Fig.16: Temperature profile for various values of Lewis number Le .

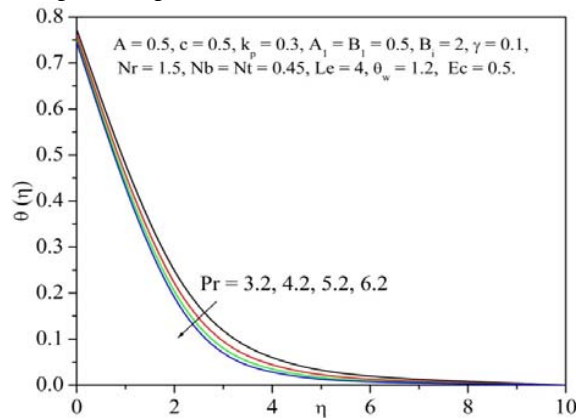


Fig.17: Temperature profile for various values of Prandtl number Pr .



Table 1: Unsteady flow with linear and nonlinear radiation values

c	k_p	A_1	B_1	B_2	Nb	Nr	Nr	γ	Ec	Pr	Lc	$A = 0.5, \theta_w = 1.2$		$A = 0.5, \theta_w = 0$	
												$\psi'(0)$	$\phi'(0)$	$\psi'(0)$	$\phi'(0)$
0												1.6026	2.5227	0.4688	2.5297
1												1.8062	1.8662	0.5564	1.8358
1.5												1.7887	1.7492	0.5542	1.7158
	0											1.8565	2.1127	0.5653	2.0879
	0.3											1.7998	2.0637	0.5483	2.0407
	0.6											1.7522	2.0226	0.5338	2.0014
		-0.5										1.9345	2.0437	0.5924	2.0139
		0										1.8671	2.0537	0.5703	2.0273
		0.5										1.7998	2.0637	0.5483	2.0407
			-0.5									1.6639	2.0778	0.5021	2.0632
			0									1.7299	2.0712	0.5245	2.0528
			0.5									1.7998	2.0637	0.5483	2.0407
				2								1.7998	2.0637	0.5483	2.0407
				5								2.1009	2.0476	0.6652	2.0113
				10								2.2178	2.0418	0.7143	1.9995
					0.2							2.0730	1.8153	0.6499	1.6960
					0.4							1.8512	2.0400	0.5675	2.0080
					0.6							1.6546	2.1088	0.4940	2.1029
						0						1.9675	2.1470	0.6090	2.1470
						0.3						1.8526	2.0861	0.5675	2.0676
						0.6						1.7500	2.0455	0.5302	2.0206
							1					1.4050	2.0652	0.5543	2.0481
							1.5					1.7998	2.0637	0.5483	2.0407
							2					2.1696	2.0642	0.5402	2.0372
								-0.2				1.8122	1.9750	0.5533	1.9491
								0				1.8037	2.0347	0.5499	2.0108
								0.2				1.7959	2.0921	0.5467	2.0701
									0.5			1.7998	2.0637	0.5483	2.0407
									1			1.5616	2.1164	0.4658	2.1120
									2			1.0957	2.2191	0.3003	2.2547
										4.2		1.6824	2.0675	0.5283	2.0362
										5.2		1.7515	2.0645	0.5409	2.0374
										6.2		1.7998	2.0637	0.5483	2.0407
											5	1.7652	2.3556	0.5340	2.3409
											10	1.6649	3.4815	0.4912	3.4918
											20	1.5787	5.0420	0.4526	5.0751



linear and nonlinear radiation values

α	t_c	A_1	B_1	B_2	Nh	Nz	Nr	γ	Ec	Dr	Le	$A = 0, \theta_w = 1.2$		$A = 0, \theta_w = 0$	
												$\theta'(0)$	$\phi'(0)$	$\theta'(0)$	$\phi'(0)$
0												1.2913	2.2406	0.3736	2.2575
1												1.3420	1.5397	0.4162	1.5234
1.5												1.2844	1.3941	0.4026	1.3743
	0											1.4938	1.8553	0.4547	1.8427
	0.3											1.3876	1.7670	0.4232	1.7573
	0.6											1.2962	1.6910	0.3961	1.6835
		-0.5										1.5810	1.7373	0.4880	1.7170
		0										1.4844	1.7521	0.4557	1.7371
		0.5										1.3876	1.7670	0.4232	1.7573
			-0.5									1.2081	1.7830	0.3629	1.7823
			0									1.2954	1.7760	0.3920	1.7714
			0.5									1.3876	1.7670	0.4232	1.7573
				2								1.3876	1.7670	0.4232	1.7573
				5								1.5712	1.7534	0.4946	1.7364
				10								1.6400	1.7484	0.5232	1.7281
					0.2							1.6568	1.5479	0.5283	1.4549
					0.4							1.4376	1.7464	0.4428	1.7291
					0.6							1.2482	1.8061	0.3687	1.8102
						0						1.5688	1.8379	0.4896	1.8381
						0.3						1.4438	1.7861	0.4439	1.7766
						0.6						1.3355	1.7512	0.4041	1.7433
							1					1.0786	1.7734	0.4229	1.7707
							1.5					1.3876	1.7670	0.4232	1.7573
							2					1.6732	1.7640	0.4195	1.7492
								-0.2				1.4033	1.6493	0.4300	1.6364
								0				1.3925	1.7293	0.4253	1.7184
								0.2				1.3830	1.8036	0.4212	1.7948
									0.5			1.3876	1.7670	0.4232	1.7573
									1			1.1240	1.8219	0.3293	1.8335
									2			0.6070	1.9292	0.1395	1.9871
										4.2		1.2915	1.7649	0.4107	1.7456
										5.2		1.3499	1.7650	0.4196	1.7503
										6.2		1.3876	1.7670	0.4232	1.7573
											5	1.3571	2.0279	0.4095	2.0258
											10	1.2756	3.0307	0.3713	3.0512
											20	1.2368	3.7853	0.3525	3.8173

Lorentzian α -Sasakian Manifold Satisfying Certain Pseudosymmetric Properties

Dr. Divyashree G.

Department of Mathematics,
Kuvempu University, Shankaraghatta - 577 451,
Shimoga, Karnataka, INDIA.
e-mail: gdivyashree9@gmail.com

Abstract: The purpose of the present paper is to study Lorentzian α -Sasakian manifold satisfying pseudo Ricci symmetric, Ricci generalized pseudo symmetric and generalized pseudo-Ricci symmetric conditions. Finally, we prove that Lorentzian α -Sasakian manifold satisfying the condition $S \cdot R=0$ reduces to Einstein manifold with scalar curvature $-\alpha^2 n(n-1)$.

Key words: Lorentzian α -Sasakian manifold, pseudo Ricci symmetric, Ricci generalized pseudo symmetric and generalized pseudo-Ricci symmetric, Ricci semisymmetric.

AMS Subject Classification: 53B30, 53C25, 53C50, 53D10.

1. Introduction:

Among the geometric properties of manifolds, symmetry is an important one and plays a significant role. Semisymmetric Riemannian manifolds was first studied by Cartan [1]. A Riemannian manifold M^n is called locally symmetric [12] if its curvature tensor R is parallel, i.e., $\nabla R = 0$. A Riemannian manifold M^n is Ricci-symmetric if its Ricci tensor S of type (0,2) satisfies $\nabla S = 0$, where ∇ denotes the Riemannian connection. A Riemannian manifold M^n is said to be semisymmetric if its curvature tensor R satisfies $R(X, Y) \cdot R = 0$, $X, Y \in T(M^n)$, where $R(X, Y)$ acts on R as a derivation [11,6].

Over the last five decades, the concept of Ricci-symmetric manifolds has been weakened by several authors to a different extent such as Ricci-recurrent

manifolds [9], Ricci semisymmetric manifolds [11], pseudo Ricci-symmetric manifolds [4] Ricci pseudo symmetric manifold [4,5].

Lorentzian manifold plays a pivotal role in differential geometric point of view because of its wide significance properties. An n -dimensional smooth differentiable manifold M with Lorentzian metric g is known as Lorentzian manifold. The idea of Lorentzian manifolds was first introduced by Matsumoto [7] in 1989. The same idea was independently studied by Mihai and Rosca [8]. A differentiable manifold M of dimension n is said to be a Lorentzian α -Sasakian manifold if it admits a (1,1)-tensor field ϕ , a vector field ξ , a 1-form η and a Lorentzian metric g which satisfy the conditions

$$\phi^2 = I + \eta \otimes \xi, \quad (1.1)$$

$$\eta(\xi) = -1, \quad \phi\xi = 0, \quad \eta(\phi X) = 0, \quad (1.2)$$

$$g(X, \xi) = \eta(X), \quad (1.3)$$

$$g(\phi X, \phi Y) = g(X, Y) + \eta(X)\eta(Y), \quad (1.4)$$

$$(\nabla_X \phi)(Y) = \alpha[g(X, Y)\xi + \eta(Y)X], \quad (1.5)$$

for all $X, Y \in T(M^n)$, where $T(M^n)$ is the Lie algebra of smooth vector fields on $T(M^n)$, α is smooth function on M^n and ∇ denotes the covariant differentiation operator of Lorentzian metric g [10,18].

On a Lorentzian α -Sasakian manifold [10,18], it can be shown that

$$\nabla_X \xi = \alpha \phi X, \quad (1.6)$$

$$(\nabla_X \eta)Y = \alpha g(\phi X, Y), \quad (1.7)$$